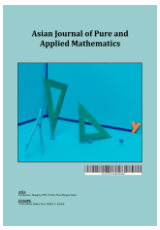

Asian Journal of Pure and Applied Mathematics

Volume 6, Issue 1, Page 253-270, 2024; Article no.AJPAM.1732

Mathematical Modelling of the Impact of Mass Concentration on Viscoelastic Fluid Flow through a Non-Porous Channel

K. W. Bunonyo [a*] and J. T. Dagana [b]

[a] MMDARG, Department of Mathematics and Statistics, Federal University Otuoke, Bayelsa State, Nigeria.
[b] Department of Mathematics and Statistics, Federal University Otuoke, Bayelsa State, Nigeria.

Authors' contributions

This work was carried out in collaboration between both authors. Both authors read and approved the final manuscript.

Article Information

Open Peer Review History:
This journal follows the Advanced Open Peer Review policy. Identity of the Reviewers, Editor(s) and additional Reviewers, peer review comments, different versions of the manuscript, comments of the editors, etc are available here: https://prh.globalpresshub.com/review-history/1732

Original Research Article

Received: 14/08/2024
Accepted: 20/10/2024
Published: 28/10/2024

Abstract

In this article, we theoretically derived a system of partial differential models representing mass concentration and momentum of viscoelastic fluid flowing through a non-porous channel in dimensional form and were further reduced to a system of ordinary differential equations using the oscillatory perturbation equations. The perturbed ordinary differential equations were solved analytically using the direct method, and the numerical simulation was performed using Wolfram Mathematica, version 12, where the physical parameters such as Schmidt number, solutal Grashof number, retardation time, and the ratio of relaxation to retardation time parameters, oscillatory frequency parameter, and mass concentration parameter were varied at a fixed period of ten units. The investigation reveals that the viscoelastic fluid velocity decreases for an increase in Schmidt number and mass concentration reaction parameter, and the velocity increases for a change in Solutal Grashof number, retardation time parameter, and the relaxation to retardation ratio parameter. In addition, the volumetric flow rate decreases for the increasing values of

**Corresponding author: E-mail: wilcoxkb@fuotuoke.edu.ng;*

Cite as: *Bunonyo, K. W., and J. T. Dagana. 2024. "Mathematical Modelling of the Impact of Mass Concentration on Viscoelastic Fluid Flow through a Non-Porous Channel". Asian Journal of Pure and Applied Mathematics 6 (1):253-70. https://jofmath.com/index.php/AJPAM/article/view/171.*

the Schmidt number and mass concentration reaction parameter; however, the flow rate increases for an increased value of the relaxation to retardation ratio. This study is important in understanding and proposing solutions to viscoelastic fluid flow challenges through a non-porous channel.

Keywords: Mathematical modelling; mass concentration; viscoelastic fluid; flow and non-porous channel.

Nomenclatures

w^* : *Dimensional velocity*
w : *Dimensionless velocity*
w_0 : *Perturbed velocity*
x^* : *Dimensional velocity*
x, y : *Dimensionless distance variables*
C^* : *Dimensional mass concentration*
ϕ : *Dimensionless mass concentration*
ϕ_0 : *Perturbed mass concentration*
Gc : *Mass Grashof number parameter*
Sc : *Schmidt number parameter*
μ_b : *Dynamic viscosity of blood*
υ : *Kinematic viscosity parameter*
λ_1 : *Ratio of relaxation to retardation parameter*
λ : *Retardation time parameter*
k_0 : *Rate of mass concentration reduction parameter*
Rd_3 : *Mass concentration reaction parameter*
ω : *Oscillatory frequency*
t : *Dimensionless time*

1 Introduction

Viscoelastic fluid is a unique type of fluid exhibits both elastic and viscous properties. It is complex and finds applications in various industries due to its unique rheological behavior, according to Galindo-Rosales et al. [1]. These fluids exhibit characteristics like turbulent drag reduction, elastic turbulence, and shear-thinning behavior, where viscosity changes significantly with shear rate. Plasma is the main component of blood and consists mostly of water, with proteins, ions, nutrients, and wastes mixed in. Red blood cells are responsible for carrying oxygen and carbon dioxide. Platelets are responsible for blood clotting. White blood cells are part of the immune system and function in immune response. According to Bunonyo et al. [2], cells and platelets make up about 45 percent of human blood, while plasma makes up the remaining 55 percent. There are several researchers who have studied the flow of blood through blood channels, and they are: Dhange et al. [3] used mathematical modelling to study the flow of blood in a stenosed artery with post-stenotic dilatation and a force field. The observed that the narrowing of an artery is caused by arteriosclerotic deposition or other aberrant tissue growth. As the growth spreads into the artery's lumen, blood flow is impeded. Research was carried out by Sriram et al. [4] to study the haematocrit dispersion in asymmetrically bifurcating vascular network topology, including vessel branching. Jones et al. [5] formulated a mathematical model for pressure losses in

the haemodialysis graft vascular circuit. In this study, they developed a mathematical model of this circuit, and pressure losses were measured in an in vitro experimental apparatus and compared with losses predicted. Elhanafy et al. [6] investigated the haematocrit variation effect on blood flow in an arterial segment with variable stenosis degree. They presented a numerical simulation of blood flow in a three-dimensional axisymmetric segment with stenosis under steady conditions. Kumawat et al. (2021) performed mathematical analysis of two-phase blood flow through a stenosed curved artery with haematocrit and temperature-dependent viscosity. A two-phase blood flow model is considered to analyse the fluid flow and heat transfer in a curved tube with time-variant stenosis. Secomb et al. (2008) investigated the theoretical models for regulation of blood flow. The study showed how blood flow rate in the normal microcirculation is regulated to meet the metabolic demands of the tissues, which vary widely with position and with time, but is relatively unaffected by changes of arterial pressure over a considerable range. Kumar et al. [7] investigated a mathematical model for blood flow through a narrow catheterised artery. The model was investigated to analyse the effect of the stenosis height, shape, catheter radius, and slip velocity on axial velocity, shear stress, and effective viscosity. Onitilo et al. [8] investigated the effects of haematocrit on blood flow through a stenosed human carotid artery; it was discovered that the resistance increases as the level of haematocrit increases. Also, the wall shear stress decreases with the increase in the haematocrit level of the red blood cells. Branigan et al. [9] researched the mean arterial pressure nonlinearity in an elastic circulatory system subjected to different haematocrits. The model was used to evaluate the equilibrium intraluminal average blood pressure in an elastic, auto-regulated arteriole-like blood vessel.

Srivastava et al. [10] formulated a theoretical model for blood flow in small vessels. A quantitative comparison shows that the model suitability represents blood flow at haematocrit (less than or equal to 40%) and in vessels up to 70 micrometres in diameter. Farina et al. [11] formulated a mathematical model for some aspects of blood microcirculation. Blood flow in vessels whose size is comparable to the RBC dimensions has very little to do with traditional fluid dynamics.

Takahashi et al. (2009) derived a mathematical model for the distribution of haemodynamic parameters in the human retinal microvascular network. Using this model, we evaluated haemodynamic parameters; including blood pressure, blood flow, and blood velocity, shears rate, and shear stress, within the retinal microcirculatory network as a function of vessel diameter. Pralhad et al. [12] carried out modelling of arterial stenosis and its applications to blood diseases. The results on shear stress and on resistance to flow for different suspensions have been shown. It was observed that the value of shear stress increases with the increase of stenosis height and decreases with the increase of couple stress parameters. Kumar et al. [13] carried out performance modelling and study of blood flow in vessels with porous effects. The study helped to understand the biofluid dynamics and flow of blood in the presence of porous effects. Ali et al. [14] researched cardiovascular dynamics through mathematical modelling of arterial blood flow. The mathematical model was solved by adopting a finite volume-based numerical technique. Kocsis et al. [15] formulated a mathematical model for the estimation of haemodynamic and oxygenation variables by tissue spectroscopy. In the study, by integrating and extending these models, they developed a general mathematical model for the estimation of haemodynamic and oxygenation variables by tissue spectroscopy. Roy et al. [16] modelled on blood flow in an artery with an unsteady overlapping stenosis: mathematical and computer modeling. The model was developed to determine the leading-order flow velocity, pressure gradient, impedance, and wall shear stress at the throats and at the critical height of the stenosis.

Khalid et al. [17] researched a review of mathematical modelling of blood flow in the human circulatory system. The study was focused on the derivation of cardiovascular system equations with the help of continuity equations and the Land Navier-Stokes equation in order to develop a general equation of normal blood flow and an extended normal blood pressure equation. Caiazzo et al. [18] carried out a mathematical modelling of blood flow in the cardiovascular system. The formulation of the mathematical modelling discussed the simulation and interplay between modelling, imaging, and experiments in order to improve clinical diagnosis and treatment.

Johnson et al. [19] researched the application of 1D blood flow models of the human arterial network to differential pressure predictions. From the study, a new use for a one-dimensional blood flow model has been

presented based on an analysis of patterns in the differences seen between pressure profiles obtained under normal (base case) and diseased (test case) conditions.

Misra et al. [20] investigated the peristaltic transport of blood in small vessels. In the study, he used the available experimental results on human blood and plotted a graph of square root of strain rate against square root of shear stress, which showed remarkable linearity with a nonzero value for the intercept on the stress axis. Gabryś et al. [21] researched blood flow simulation through fractal models of the circulatory system. The study shows that the model of the blood vessel system is a certain geometrical simplification, but it suffices for acceptable blood flow analysis. Tawhai et al. [22] formulated a model for pulmonary blood flow. The study focusses on computational models that have been developed to study the different mechanisms contributing to regional perfusion of the lung. Tsubota et al. [23] carried out a simulation study on effects of haematocrit on blood flow properties using the particle method. As a result, it was shown that at higher haematocrit, RBCs were less deformed into a parachute shape during their downstream motion, indicating that mechanical interaction between RBCs restricted the RBC deformation.

Kehrer et al. [24] formulated the development of cerebral blood flow volume in preterm neonates during the first two weeks of life. The study helped to investigate the postnatal development of cerebral perfusion in preterm neonates with normal brains by serial measurements during the first 14 days of life. Haddy et al. [25] researched the role of potassium in regulating blood flow and blood pressure. The study revealed that, when blood is infused into the arterial supply of a vascular bed, blood flow increases. Kershen et al. (2002) modelled on blood flow, pressure, and compliance in the male human bladder. The study shows that human bladder blood flow tends to increase with increasing volume and pressure and depends largely on local regulation. Liao et al. (2013) researched skin blood flow dynamics and its role in pressure ulcers. It shows that blood flow over large areas of skin can be measured using laser Doppler imaging, and rapid dynamic changes in flow over a small area can be measured using laser Doppler flowmetry. Goodwill et al. [26] formulated a regulation of coronary blood flow. It regulates with emphasis on functional anatomy and the interplay between the physical and biological determinants of myocardial oxygen delivery. The flow of viscoelastic fluids through porous media has attracted the attention of a large number of scholars owing to their application in the fields of extraction of energy from geothermal regions and in the flow of oil through porous rocks. Many common liquids, such as certain paints, polymer solutions, some organic liquids, and many new materials of industrial importance, exhibit both viscous and elastic properties. Fluids with such characteristics are called viscoelastic fluids.

The aim of this research is to investigate the impact of mass concentration on the flow of viscoelastic fluid through a non-porous channel. Proffer an analytical solution as an expression for the mass concentration and the velocity profile, the volumetric flow rate, and the rate of mass transfer through the channel, and present the results graphically.

2 Mathematical Formulation and Method of Solution

Before formulating mathematical models that represent mass concentration and its effect on viscoelastic fluid flowing through a non-porous channel, let's consider the following assumptions:

2.1 Mathematical formulation

In formulating mathematical models representing the situation under investigation, let's consider the following assumptions:

1. The fluid is considered to be viscoelastic due to the formed elements composition and insoluble and Tran's fats in it.
2. There is an impact of mass in mass concentration in the fluid, thereby causing the fluid to exhibits both elastic and viscous characteristics.
3. The flow is through a non-porous channel
4. The flow obeys the principle of no-slip

5. The impact of magnetic field is neglected and the flow is towards the axial direction
6. There is relaxation and retardation time effect on the flow momentum
7. The rate of mass reaction reduction affecting the both the mass concentration and fluid velocity profiles

In view of the above mentioned assumptions, we present the diagram showing the flow of viscoelastic fluid through a non-porous channel without the impact of magnetic field and it obeys the no-slip boundary condition.

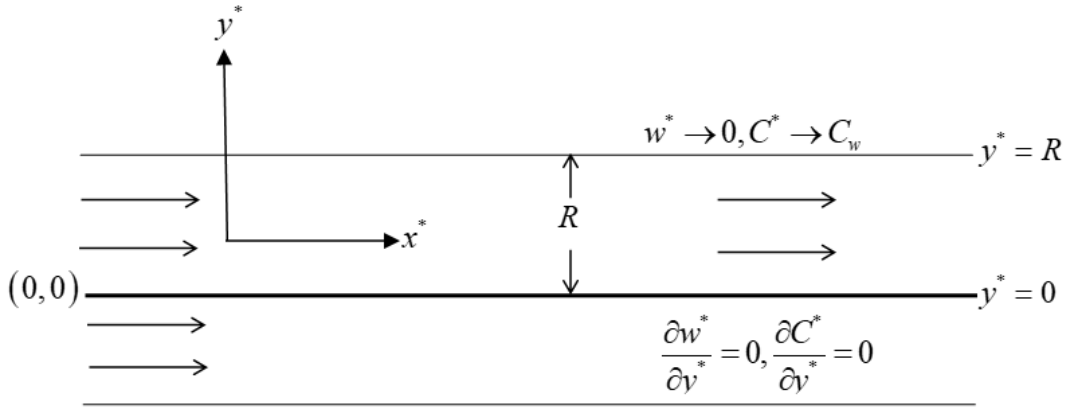

Fig. 1. Diagram showing the flow of viscoelastic fluid through a non-porous channel

Following the aforementioned assumptions and Bunonyo et al. (2020), Butter et al. (2024) we present the derived models governing the mass concentration and viscoelastic fluid flow with the corresponding boundary conditions as follows:

2.2 Method of solution

In this section, we are going to present the models governing the mass concentration and the effect on the viscoelastic fluid flowing through the non-porous channel.

2.2.1 Momentum equation with the impact of mass concentration

In order to understand the role of relaxation and retardation time fact, we modified the governing models from previous research by Bunonyo *et al*' [27], hence the new model governing the momentum of the viscoelastic fluid flowing through the non-porous channel is:

$$\rho_b \frac{\partial w^*}{\partial t^*} = \frac{\mu_b}{1+\lambda_1}\left(1+\lambda_2 \frac{\partial}{\partial t^*}\right)\frac{\partial^2 w^*}{\partial y^{*2}} + \rho_b g \beta_C \left(C^* - C_\infty\right) \tag{1}$$

2.2.2 Mass concentration equation

The mass concentration equation is derived from Bunonyo et al. (2021)

$$\frac{\partial C^*}{\partial t^*} = D_m \frac{\partial^2 C^*}{\partial y^{*2}} - k_0 \left(C^* - C_\infty\right) \tag{2}$$

The corresponding boundary conditions are as:

$$\left.\begin{aligned} &\frac{\partial w^*}{\partial y^*}=0,\frac{\partial C^*}{\partial y^*}=0 \ \text{ at } \ y^*=0 \\ &w^*\to 0, C^*\to C_w \ \text{ at } \ y^*\to R \end{aligned}\right\} \tag{3}$$

2.2.3 Dimensional parameters

In order to make the governing equations dimensionless, we shall introduce the following scaling quantities derived from Bunonyo et al. (2021), they are:

$$\left.\begin{aligned} &\phi=\frac{C^*-C_\infty}{C_w-C_\infty}, Gc=\frac{g\beta_C\left(C_w-C_\infty\right)R_0^3}{\upsilon^2}, Rd_3=\frac{k_r R_0^2}{\upsilon}, \\ &x=\frac{x^*}{\lambda_0}, y=\frac{y^*}{R_0}, w=\frac{w^* R_0}{\upsilon}, t=\frac{\upsilon t^*}{R_0^2}, \lambda=\frac{\lambda_2\upsilon}{R_0^2}, Sc=\frac{\upsilon}{D_m} \end{aligned}\right\} \tag{4}$$

The governing equations (1)-(4) are reduced using equation (4), the dimensionless governing equations are as follows:

$$\frac{\partial w}{\partial t}=\left(\frac{1}{1+\lambda_1}\right)\left(1+\lambda\frac{\partial}{\partial t}\right)\frac{\partial^2 w}{\partial y^2}+Gc\phi \tag{5}$$

$$\frac{\partial \phi}{\partial t}=\frac{1}{Sc}\frac{\partial^2\phi}{\partial y^2}-Rd_3\phi \tag{6}$$

The corresponding boundary conditions are as:

$$\left.\begin{aligned} &\frac{\partial w}{\partial y}=0,\frac{\partial \phi}{\partial y}=0 \ \text{ at } \ y=0 \\ &w\to 0,\phi\to 1 \quad \text{at } \ y\to h \end{aligned}\right\} \tag{7}$$

3 Analytical Solution

We consider that the flow is being generated by an oscillatory condition; hence the dimensionless equations can be represented as:

$$\left.\begin{aligned} &w\left(y,t\right)=w_0 e^{\omega t} \\ &\phi\left(y,t\right)=\phi_0 e^{\omega t} \end{aligned}\right\} \tag{8}$$

Substituting equation (8) into the dimensionless governing equations (5)-(7), they are reduced to:

$$\frac{d^2 w_0}{dy^2} - \frac{\omega(1+\lambda_1)}{1+\lambda\omega} w_0 + \frac{Gc(1+\lambda_1)}{1+\lambda\omega}\phi_0 = 0 \tag{9}$$

$$\frac{d^2 \phi_0}{dy^2} - (Rd_3 + \omega) Sc\phi_0 = 0 \tag{10}$$

Let $\beta_1^2 = \frac{\omega(1+\lambda_1)}{(1+\lambda\omega)}, Gc_1 = \frac{Gc(1+\lambda_1)}{(1+\lambda\omega)}$, and $\beta_3^2 = (Rd_3 + \omega) Sc$ so that equations (9) and (10) reduces to:

$$\frac{d^2 w_0}{dy^2} - \beta_1^2 w_0 + Gc_1\phi_0 = 0 \tag{11}$$

$$\frac{d^2 \phi_0}{dy^2} - \beta_3^2\phi_0 = 0 \tag{12}$$

The corresponding boundary conditions are as:

$$\left.\begin{aligned} &\frac{dw_0}{dy} = 0, \frac{d\phi_0}{dy} = 0 \quad \text{at } y = 0 \\ &w_0 \to 0, \phi_0 \to e^{-\omega t} \quad \text{at } y \to h \end{aligned}\right\} \tag{13}$$

Solving equation (12), we have:

$$\phi_0(y) = A\sinh(\beta_3 y) + B\cosh(\beta_3 y) \tag{14}$$

Solving equation (14) using equation (13), we have:

$$\phi_0(y) = \frac{\cosh(\beta_3 y)}{\cosh(\beta_3 h)} e^{-\omega t} \tag{15}$$

Substituting equations (15) into equation (8), this is:

$$\frac{d^2 w_0}{dy^2} - \beta_1^2 w_0 = -\frac{Gc_1 e^{-\omega t}}{\cosh(\beta_3 h)}\cosh(\beta_3 y) \tag{16}$$

Let $\beta_6 = -\frac{Gc_1 e^{-\omega t}}{cosh(\beta_3 h)}$, so that equation (16) becomes:

$$\frac{d^2 w_0}{dy^2} - \beta_1^2 w_0 = \beta_6 cosh(\beta_3 y) \tag{17}$$

Solving equation (17), we have:

$$w_{0h} = c_9 sinh(\beta_1 y) + c_{10} cosh(\beta_1 y) \tag{18}$$

The particular part of equation (17) is

$$w_{0p} = \left(\frac{\beta_6}{\beta_3^2 - \beta_1^2}\right) cosh(\beta_3 y) \tag{19}$$

$$w_0 = c_9 sinh(\beta_1 y) + c_{10} cosh(\beta_1 y) + \left(\frac{\beta_6}{\beta_3^2 - \beta_1^2}\right) cosh(\beta_3 y) \tag{20}$$

Simplifying equation (20) using the boundary conditions in equation (13), we have:

$$w_0 = \left(\frac{\beta_6}{\beta_1^2 - \beta_3^2}\right) \frac{cosh(\beta_3 h)}{cosh(\beta_1 h)} cosh(\beta_1 y) + \left(\frac{\beta_6}{\beta_3^2 - \beta_1^2}\right) cosh(\beta_3 y) \tag{21}$$

Substituting equations (21) and (15) into equation (8), we have:

$$\phi(y,t) = \frac{cosh(\beta_3 y)}{cosh(\beta_3 h)} \tag{22}$$

$$w(y,t) = \left(\left(\frac{\beta_6}{\beta_1^2 - \beta_3^2}\right) \frac{cosh(\beta_3 h)}{cosh(\beta_1 h)} cosh(\beta_1 y) + \left(\frac{\beta_6}{\beta_3^2 - \beta_1^2}\right) cosh(\beta_3 y)\right) e^{\omega t} \tag{23}$$

3.1 The volumetric flow rate within the channel

In order to calculate the flow rate of the viscoelastic fluid in the channel, we shall state the flow rate mathematically as:

$$Q = \int_{y=0}^{y=h} w_0 dy \tag{24}$$

Substituting the equation (21) into equation (24) and integrate, we have:

$$Q = \int_{y=0}^{y=h} \left(\left(\frac{\beta_6}{\beta_1^2 - \beta_3^2} \right) \frac{cosh(\beta_3 h)}{cosh(\beta_1 h)} cosh(\beta_1 y) + \left(\frac{\beta_6}{\beta_3^2 - \beta_1^2} \right) cosh(\beta_3 y) \right) dy \tag{25}$$

Simplifying equation (25), we have:

$$Q = \left(\frac{1}{\beta_1} \left(\frac{\beta_6}{\beta_1^2 - \beta_3^2} \right) \frac{cosh(\beta_3 h)}{cosh(\beta_1 h)} sinh(\beta_1 y) + \frac{1}{\beta_3} \left(\frac{\beta_6}{\beta_3^2 - \beta_1^2} \right) sinh(\beta_3 y) \right)_{y=0}^{y=h} \tag{26}$$

Simplifying equation (26), we have:

$$Q = \frac{1}{\beta_1} \left(\frac{\beta_6}{\beta_1^2 - \beta_3^2} \right) \frac{cosh(\beta_3 h)}{cosh(\beta_1 h)} sinh(\beta_1 h) + \frac{1}{\beta_3} \left(\frac{\beta_6}{\beta_3^2 - \beta_1^2} \right) sinh(\beta_3 h) \tag{27}$$

3.2 The shear stress with the channel

$$\chi_h = \left. \frac{\partial w_0}{\partial y} \right|_{y=h} \tag{28}$$

Simplifying equation (28) using equation (21), we have:

$$\chi_h = \left(\frac{\beta_1 \beta_6}{\beta_1^2 - \beta_3^2} \right) \frac{cosh(\beta_3 h)}{cosh(\beta_1 h)} sinh(\beta_1 h) + \left(\frac{\beta_3 \beta_6}{\beta_3^2 - \beta_1^2} \right) sinh(\beta_3 h) \tag{29}$$

4 Results and Discussion

In this section we shall be presenting the graphical results obtained from the simulation in the preceding sections. The dataset for the parameters used in the simulation are the range of values within the set: $\lambda = \{1,3,5,7,9\}, \lambda_1 = \{2,4,6,8,10\}, Gc = \{5,10,15,20,25\}, Sc = \{2,4,6,8,10\}$ and the mass reduction parameter values are $Rd_3 = \{0.3,0.6,0.9,1.2,1.5\}$, obtained from previous results by Bunonyo et al. [27], and the graphical results are presented as:

Following the numerical simulation after varying the various pertinent biophysical parameters, we shall discuss the results in the above section for Fig. 2, [28] for the velocity of the viscoelastic fluid and the mass concentration above.

Fig. 2 illustrate the impact of Schmidt number on the velocity of non-viscous viscoelastic fluid, and the figure is of the view that, increase in Schmidt number decreases the velocity from the maximum velocity of 414.409 to zero when the boundary layer attains its maximum, while the other pertinent parameters and their values are $Rd_3 = 0.3, Gc = 15, \lambda = 3, \lambda_1 = 10, t = 10$. Fig. 3 depicts the impact of mass reaction values on the velocity of non-viscous viscoelastic fluid. This results if of the view that increase mass reaction decreases the fluid velocity. Because we noticed that the velocity was at maximum of 414.409 when $Rd_3 = 0.3$, however,

the velocity continue to decreases as the mass reaction values increases, and the other pertinent parameters and their values remains at $Sc = 2, Gc = 15, \lambda = 3, \lambda_1 = 10, t = 10$.

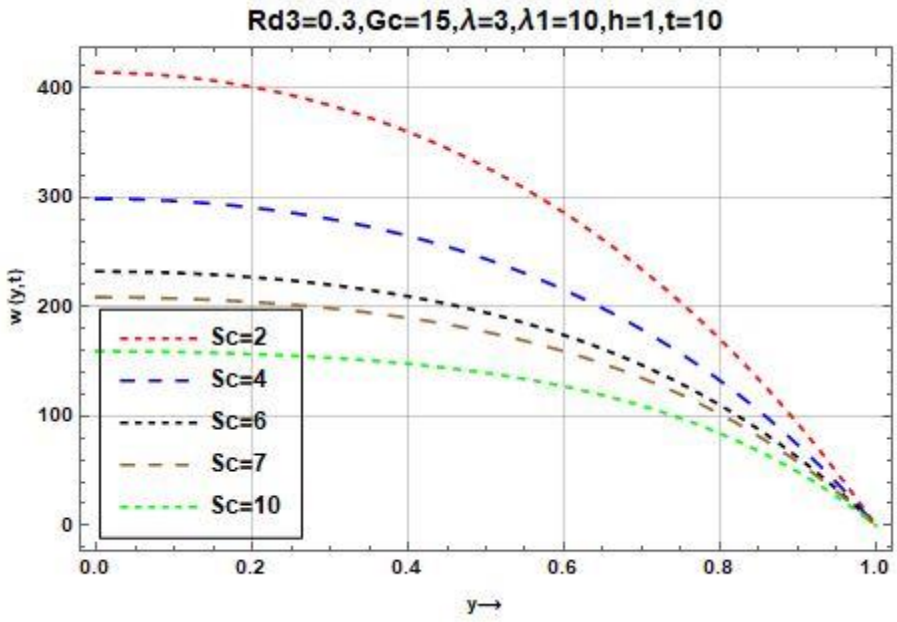

Fig. 2. Plot showing the impact of Schmidt number on the velocity of viscoelastic fluid through a non-porous channel

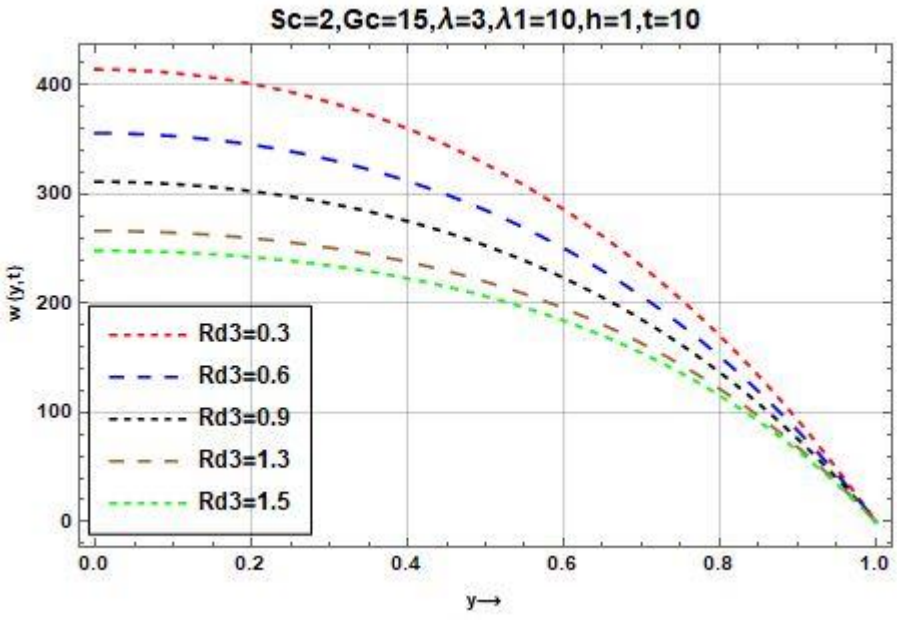

Fig. 3. Plot showing the impact of mass concentration on the velocity of viscoelastic fluid through a non-porous channel

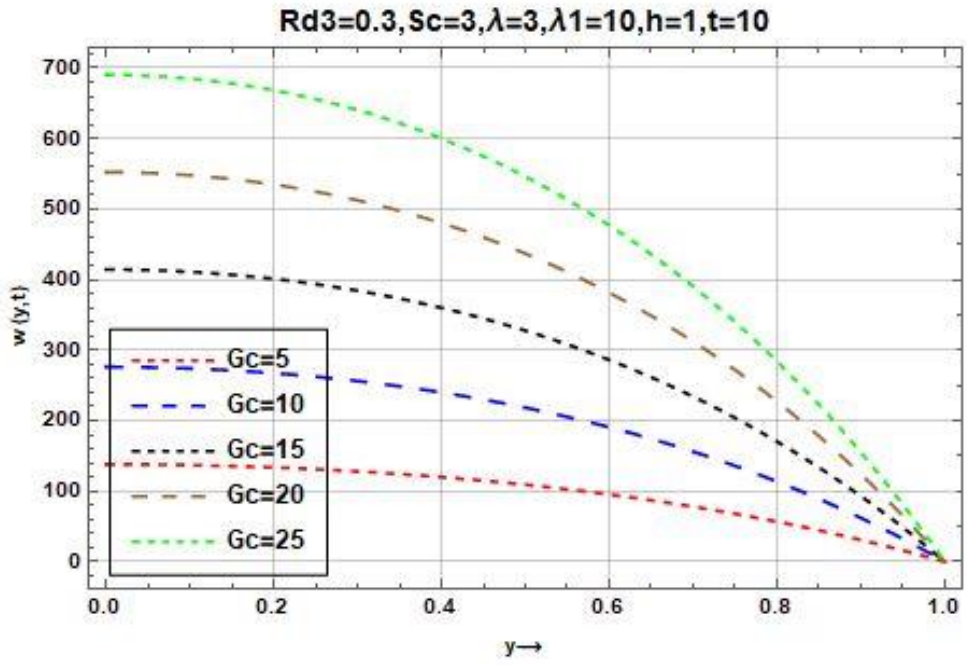

Fig. 4. Plot showing the impact of solutal Grashof number on the velocity of viscoelastic fluid through a non-porous channel

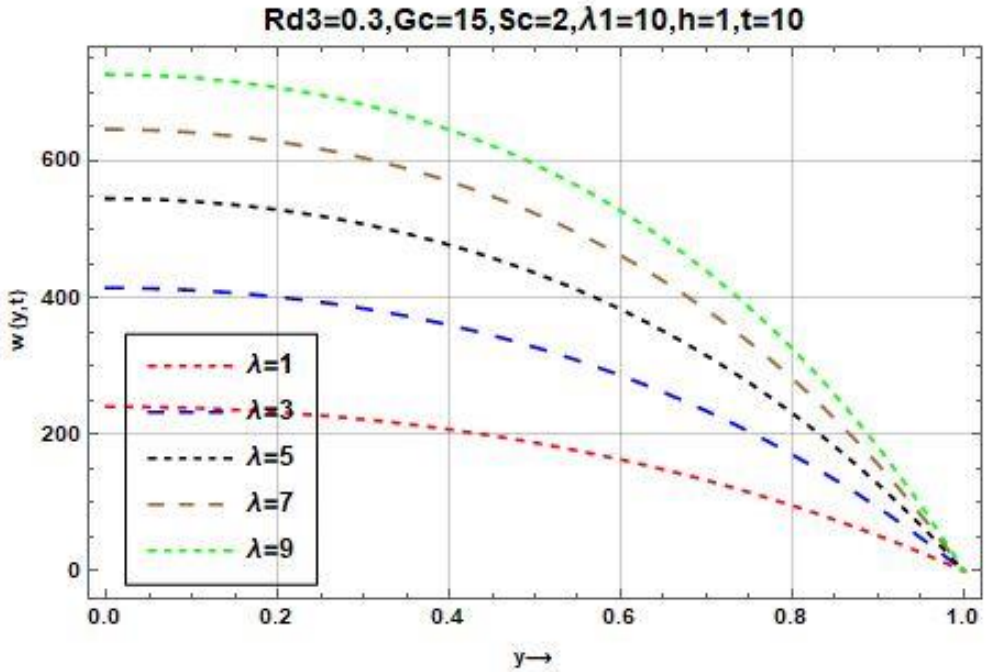

Fig. 5. Plot showing the impact of retardation time on the velocity of viscoelastic fluid through a non-porous channel

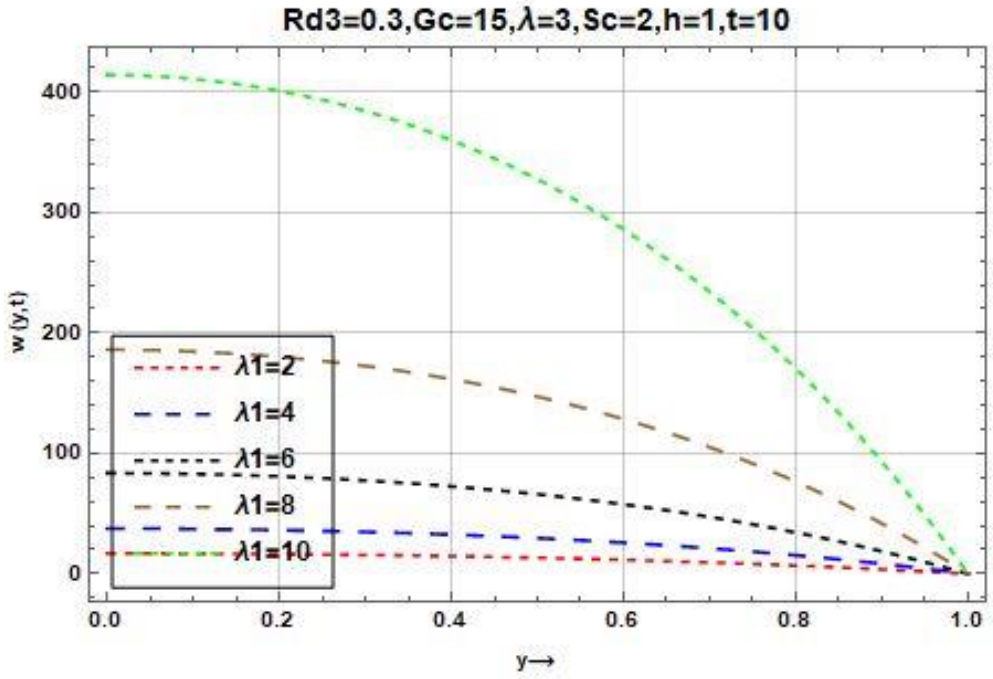

Fig. 6. Plot showing the impact of relaxation to retardation ratio on the velocity of viscoelastic fluid through a non-porous channel

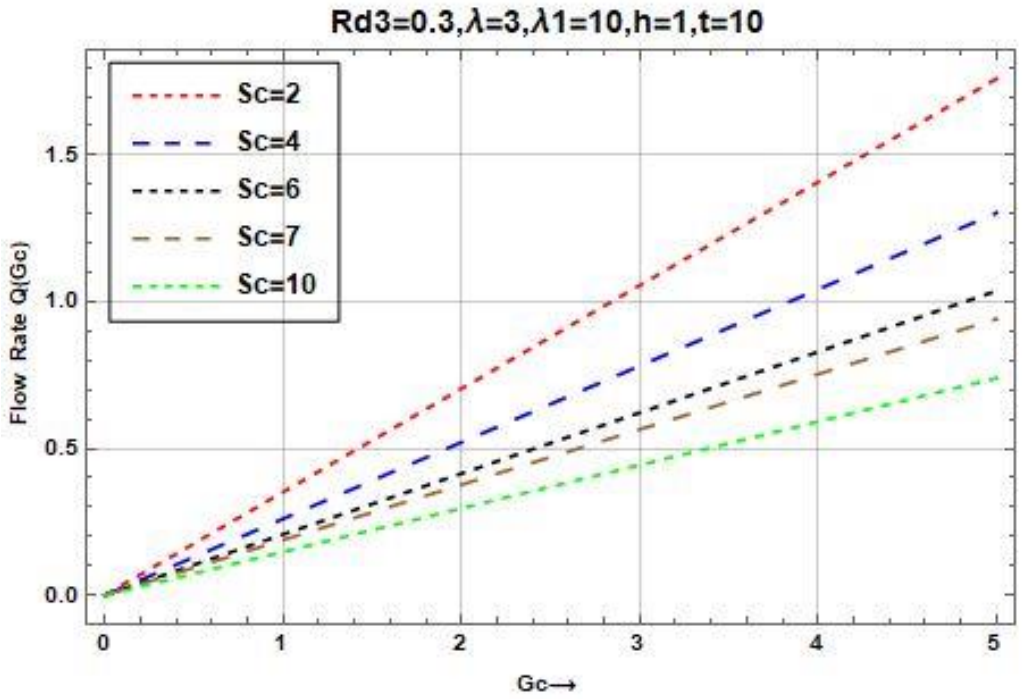

Fig. 7. Plot showing the impact of Schmidt number on flow rate against the mass Grashof number

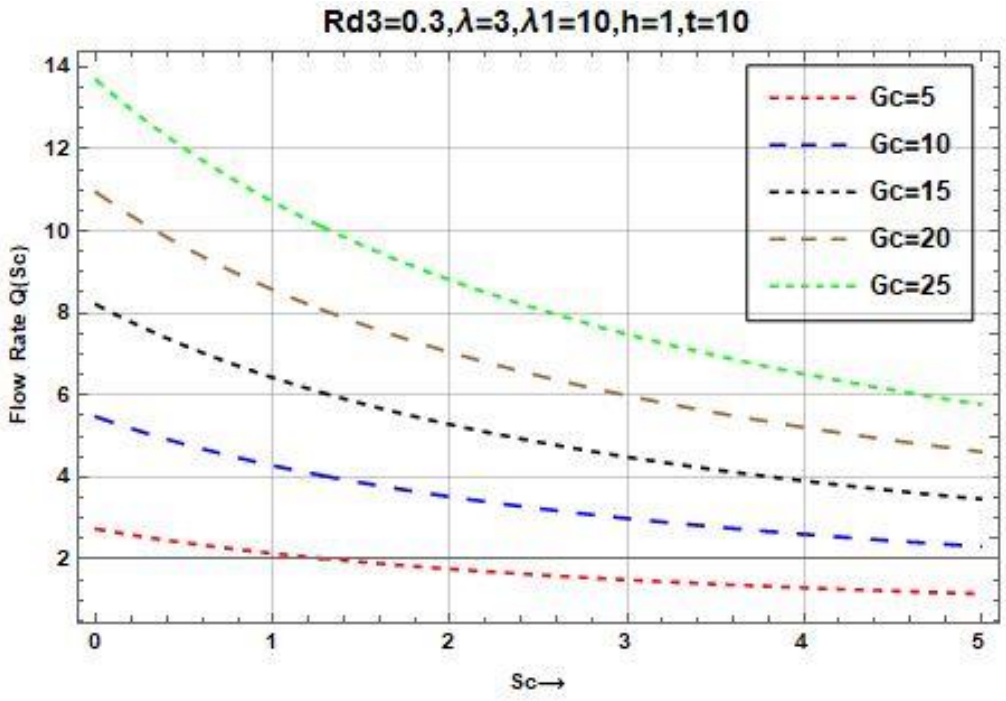

Fig. 8. Plot showing the impact of mass Grashof number on flow rate against the Schmidt number

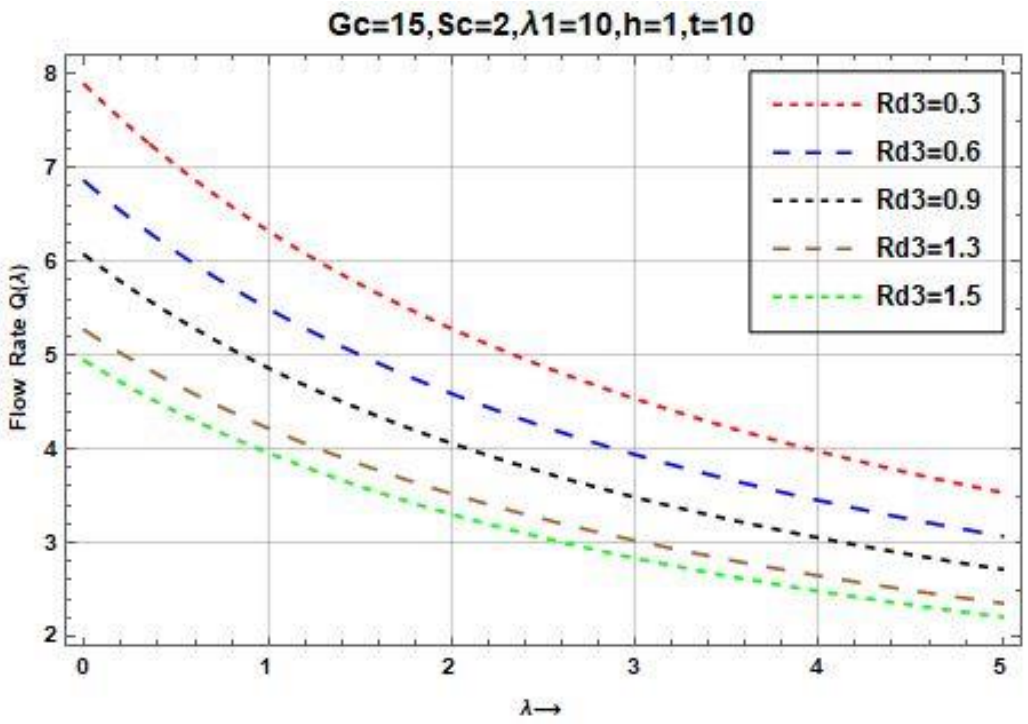

Fig. 9. Plot showing the impact of mass reduction on flow rate against retardation parameter

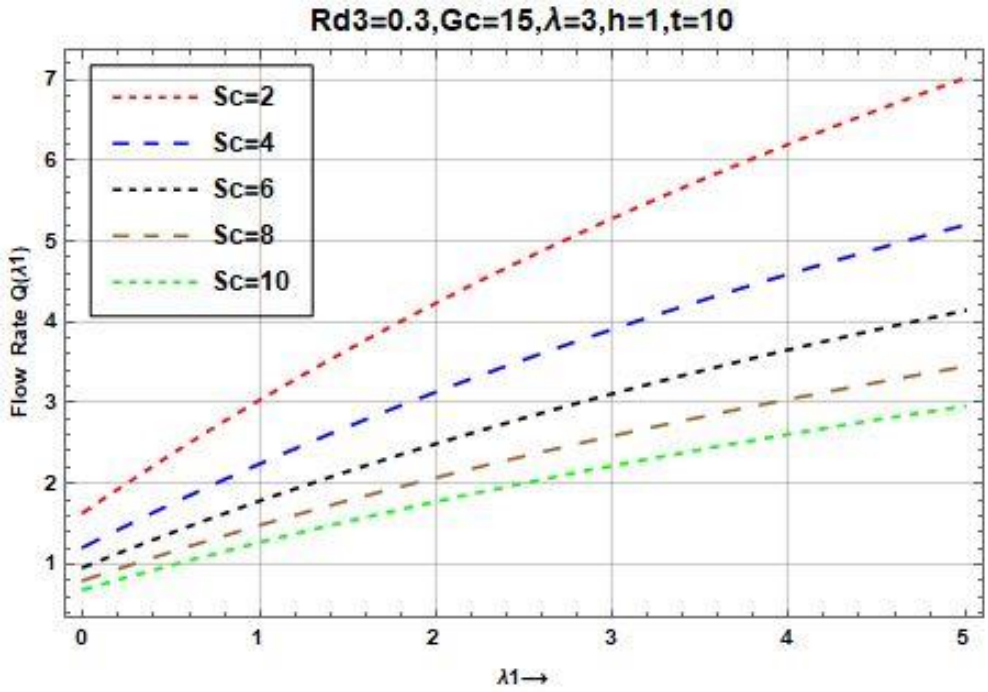

Fig. 10. Plot showing the impact of Schmidt number on flow rate against relaxation to retardation ratio

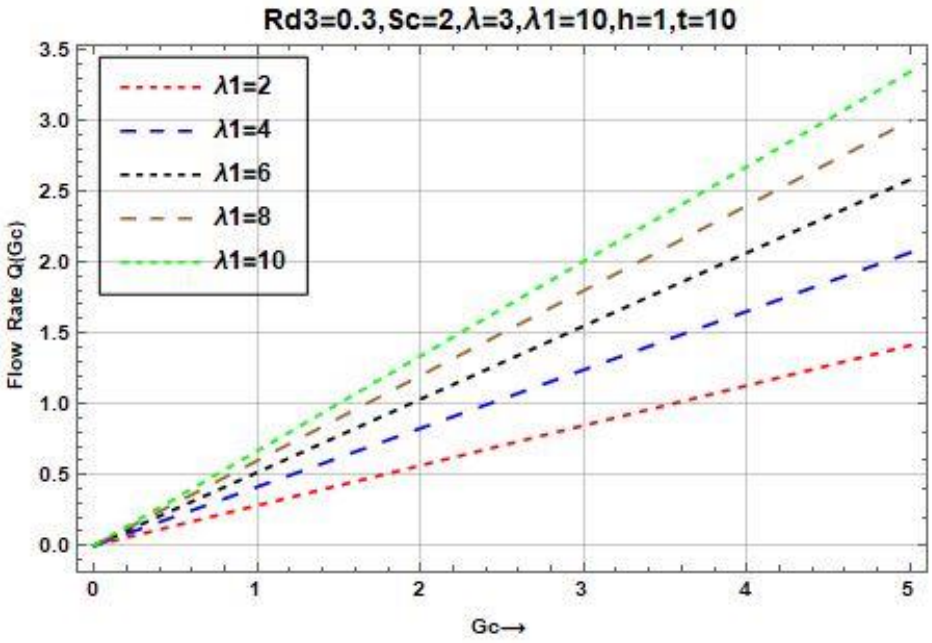

Fig. 11. Plot showing the impact of relaxation to retardation ratio on the flow rate against the mass Grashof number

Fig. 4 illustrate the impact of Schmidt number on the velocity of non-viscous viscoelastic fluid, and the figure is of the view that an increase in Schmidt number decreases the velocity from the maximum velocity of

414.409 to zero when the boundary layer attains its maximum, while the other pertinent parameters and their values are $Rd_3 = 0.3, Gc = 15, \lambda = 3, \lambda_1 = 10, t = 10$. Fig. 5 showing the impact of retardation time on the velocity of non-viscous viscoelastic fluid, where it is seen that the velocity of the fluid increases for different values of the retardation time from $\lambda = 1, 3, 5, 7, 9$. However, we noticed that the fluid velocity attained different maximum at the centre of the channel before decreasing to zero at maximum boundary layer thickness, and the other pertinent parameters and their values remains at $Sc = 2, Gc = 15, \lambda = 3, \lambda_1 = 10, t = 10$.

Fig. 6 illustrate the impact of relaxation to retardation ratio on the velocity of the non-viscous viscoelastic fluid. The result indicates that the relaxation to retardation was minimum at 16.8922 units but increases gradually to 414.409 units for the increasing values of the relaxation to retardation ration. Fig. 7 illustrates the impact of Schmidt number on the flow rate against the solutal Grashof number. And the result showed that the flow rate decreases for an increase in Schmidt number. The impact of the solutal Grashof number on the volumetric flow rate was investigated and the result shown in Fig. 8. The plot showed that the flow rate increases against the Schmidt number for an increasing value of the solutal Grashof number $Gc = 5, 10, 15, 20, 25$, while the other pertinent parameters remained the same $Rd_3 = 0.3, \lambda = 3, \lambda_1 = 10, h = 1, t = 10$. The flow rate against retardation parameter was investigated and result shown in Fig. 9 and the figure depicts that the flow rate decreases against the retardation parameter for an increasing values of the mass reaction parameter.

Fig. 10 depicts a scenario where the flow rate decreases against the relaxation to retardation ratio increase while every other parameter quantities remain the same.

Fig. 11 illustrated that the flow rate increases against the solutal Grashof number as the impact of the relaxation to retardation ratio from $\lambda_1 = 2, 4, 6, 8, 10$ on the flow increases.

5 Conclusion

The numerical simulation was carried out to investigate the impact of the pertinent values for the different parameters on the viscoelastic fluid and flow rate of the viscoelastic fluid through the non-porous channel after solving for the flow profile analytically, we can conclude as follows:

- The velocity profile of the viscoelastic fluid decreases for an increase in Schmidt number
- The velocity profile of the viscoelastic fluid decreases for different values of mass reaction parameter
- The velocity profile of the viscoelastic fluid increases for different values of the solutal Grashof number
- The velocity profile viscoelastic fluid increases for different values of the retardation time parameter
- The velocity profile viscoelastic fluid increases for different values of the relaxation to retardation ratio parameter
- The flow rate decreases for different values of the Schmidt number
- We noticed an increase in volumetric flow rate for different values of the solutal Grashof number
- We noticed a flow rate decreases for different values of the mass reduction parameter
- The volumetric flow rate was observed to have decreased for different values of the Schmidt number
- The flow rate increases for different values of relaxation to retardation ratio.

6 Future Work

This research is part of an ongoing study to investigate the effect of mass concentration and heat absorption on the non-viscous viscoelastic fluid flowing through porous or non-porous blood vessels.

Disclaimer (Artificial Intelligence)

Author(s) hereby declare that NO generative AI technologies such as Large Language Models (ChatGPT, COPILOT, etc.) and text-to-image generators have been used during the writing or editing of this manuscript.

Competing Interests

Authors have declared that no competing interests exist.

References

[1] Galindo-Rosales FJ, Campo-Deano L, Pinho FT, Van Bokhorst E, Hamersma PJ, Oliveira MS, Alves MA. Microfluidic systems for the analysis of viscoelastic fluid flow phenomena in porous media. Microfluidics and Nanofluidics. 2012;12:485-498.

[2] Bunonyo KW, Butter JK, Eli IC. Modelling and simulation of the effect of prandtl and soret numbers on mass concentration with magnetic intensity in a blood channeL; 2024.

[3] Dhange M, Sankad G, Safdar R, Jamshed W, Eid MR, Bhujakkanavar U, Chouikh R. A mathematical model of blood flow in a stenosed artery with post-stenotic dilatation and a forced field. Plos One. 2022;17(7):e0266727.

[4] Sriram K, Intaglietta M, Tartakovsky DM. Hematocrit dispersion in asymmetrically bifurcating vascular networks. American Journal of Physiology-Heart and Circulatory Physiology. 2014;307(11):H1576-H1586.

[5] Jones SA, Jin S, Kantak A, Bell DA, Paulson WD. Mathematical model for pressure losses in the hemodialysis graft vascular circuit. J. Biomech. Eng. 2005;127(1):60-66.

[6] Elhanafy A, Elsaid A, Guaily A. Numerical investigation of hematocrit variation effect on blood flow in an arterial segment with variable stenosis degree. Journal of Molecular Liquids. 2020;313:113550.

[7] Kumar H, Chandel RS, Kumar S, Kumar S. A mathematical model for blood flow through a narrow catheterized artery. Intl J. Theoret. Appl. Sci. 2013;5(2):101-108.

[8] Onitilo S, Usman M, Daniel D. Effects of hematocrit on blood flow through a stenosed human carotid artery. Iraqi Journal of Science. 2020;2106-2114.

[9] Branigan T, Bolster D, Vázquez BYS, Intaglietta M, Tartakovsky DM. Mean arterial pressure nonlinearity in an elastic circulatory system subjected to different hematocrits. Biomechanics and Modeling in Mechanobiology. 2011;10:591-598.

[10] Srivastava VP. A theoretical model for blood flow in small vessels. Applications and Applied Mathematics: An International Journal (AAM). 2007;2(1):5.

[11] Farina A, Fasano A, Rosso F. Mathematical models for some aspects of blood microcirculation. Symmetry. 2021;13(6):1020.

[12] Pralhad RN, Schultz DH. Modeling of arterial stenosis and its applications to blood diseases. Mathematical Biosciences. 2004;190(2):203-220.

[13] Kumar A, Varshney CL, Singh VP. Performance modeling and study of blood flow in vessels with porous effects. Applied Mathematics. 2012;2(5):166-170.

[14] Ali S, Najjar IMR, Sadoun AM, Fathy A. Navigating cardiovascular dynamics through mathematical modeling of arterial blood flow. Ain Shams Engineering Journal. 2024;15(4):102594.

[15] Kocsis L, Herman P, Eke A. Mathematical model for the estimation of hemodynamic and oxygenation variables by tissue spectroscopy. Journal of Theoretical Biology. 2006;241(2):262-275.

[16] Roy R, Riahi DN. On blood flow in an artery with an unsteady overlapping stenosis: mathematical and computer modeling. International Journal of Fluid Mechanics Research. 2013;40(1).

[17] Khalid AK, Othman ZS, Shafee CM. A review of mathematical modelling of blood flow in human circulatory system. In Journal of Physics: Conference Series IOP Publishing. 2021;1988(1):012010.

[18] Caiazzo A, Vignon-Clementel IE. Mathematical modeling of blood flow in the cardiovascular system. Quantification of Biophysical Parameters in Medical Imaging. 2018;45-70.

[19] Johnson DA, Rose WC, Edwards JW, Naik UP, Beris AN. Application of 1D blood flow models of the human arterial network to differential pressure predictions. Journal of Biomechanics. 2011;44(5):869-876.

[20] Misra JC, Pandey SK. Peristaltic transport of blood in small vessels: Study of a mathematical model. Computers & Mathematics with Applications. 2002;43(8-9):1183-1193.

[21] Gabryś E, Rybaczuk M, Kędzia A. Blood flow simulation through fractal models of circulatory system. Chaos, Solitons & Fractals. 2006;27(1):1-7.

[22] Tawhai MH, Burrowes KS. Modelling pulmonary blood flow. Respiratory physiology & Neurobiology. 2008;163(1-3):150-157.

[23] Tsubota KI, Wada S, Yamaguchi T. Particle method for computer simulation of red blood cell motion in blood flow. Computer Methods and Programs in Biomedicine. 2006;83(2):139-146.

[24] Kehrer M, Blumenstock G, Ehehalt S, Goelz R, Poets C, Schöning M. Development of cerebral blood flow volume in preterm neonates during the first two weeks of life. Pediatric Research. 2005;58(5):927-930.

[25] Haddy FJ, Vanhoutte PM, Feletou M. Role of potassium in regulating blood flow and blood pressure. American Journal of Physiology-Regulatory, Integrative and Comparative Physiology. 2006; 290(3), R546-R552.

[26] Goodwill AM, Szoeke C. A systematic review and meta-analysis of the effect of low vitamin D on cognition. Journal of the American Geriatrics Society. 2017;65(10):2161-2168.

[27] Bunonyo KW, Amos E. Theoretical investigation of the role of perfusion rate and haematocrit on blood flow and its impact on radiation behavior of tissue for tumor treatment. Theoretical Mathematics and Applications. 2020;10(3):27-58.

[28] Butter JK, Bunonyo KW, Eli IC. Mathematical modelling of the thermosolutal effect on blood flow through a micro-channel in the presence of a magnetic field. British Journal of Multidisciplinary and Advanced Studies. 2024;5(4):14-32.

Peer-review history:
The peer review history for this paper can be accessed here (Please copy paste the total link in your browser address bar)
https://prh.globalpresshub.com/review-history/1732